Low-Energy Scattering of Electrons by Helium

P. G. Burke*
School of Physics and Applied Mathematics, Queens University, Belfast, Ireland

and

J. W. Cooper
National Bureau of Standards, Washington, D.C. 20234

and

S. Ormonde†
Quantum Systems, Inc., Albuquerque, New Mexico 87108

(Received 4 February 1969)

The close-coupling equations for electron-helium scattering have been solved in the energy range near the $n=2$ thresholds. Cross sections for elastic scattering from both ground and excited states, for excitation of the ground state to the $n=2$ states ($2\,^3S$, $2\,^1S$, $2\,^3P$, and $2\,^1P$), and for excitation and de-excitation processes involving only the $n=2$ levels are presented and compared with experimental evidence on total metastable production, on angular distributions of excitation cross sections to the $n=2$ levels, and on processes involving only the $n=2$ states. The percentage polarization of light emitted by electron-impact excitation to the $2\,^3P$ and $2\,^1P$ states is computed and compared with experiment. The calculations indicate the importance of resonances in near threshold excitation and de-excitation processes in He. An attempt has been made to understand the resonant structure by considering both the energy dependence of the eigenphases of the many-channel S matrix produced by solving the close-coupling equations and the energy dependence of eigenvalues of the related time-delay matrix.

I. INTRODUCTION

Low-energy scattering of electrons by helium has been carried out experimentally for roughly the past 50 years. As of 1952 the total and differential scattering cross sections for elastic scattering had been measured by several investigators. The results led to the realization of the important influence of polarization and exchange effects on these cross sections.[1] It was also realized that calculations for inelastic scattering processes at near threshold energies would be difficult to carry out.

Experiments performed since the early 1950's on helium have considerably aided our understanding of low-energy electron scattering processes. A measurement of the total metastable production near threshold[2] led to the conjecture[3] that short-lived resonant states had an appreciable effect on the scattering process in the vicinity of the thresholds for inelastic processes. The discovery of a resonance in elastic scattering for helium[4] is the first in a series of discoveries that have shown that resonant phenomena are the rule rather than the exception in low-energy electron scattering processes.[5]

On the theoretical side numerous attempts have been made in recent years to calculate both elastic and inelastic scattering cross sections for helium. Considerable progress has been made in refining the already good agreement between theory and experiment for elastic scattering by improved methods of approximation.[6] On the other hand, attempts at estimating inelastic scattering cross sections near threshold[7-9] have met with mixed success presumably because the important role that polarization effects and resonances play in near threshold excitation processes was not fully realized.

In this paper we present the results of a series of calculations intended specifically to explore the role of resonances on the scattering process in the vicinity of the $n=2$ thresholds of He.[10] The method of calculation is close coupling, i.e., an expansion of the full three electron wave function describing the helium atom plus electron in terms of the wave functions of the lowest five states of the helium atom. In this respect our method is similar to recent work on two-electron systems[11] with the added complication that the states of the helium atom must first be approximated in order to carry out the expansion. Our work may also be considered as an extension of the work of Ref. 9 to include all four of the $n=2$ states of helium in the expansion, an extension which, as we will see, has a profound effect on the resonant structure of the cross sections for low-energy scattering processes. The use of a five state expansion

enables us to calculate in one fell swoop the cross sections for 15 elastic and inelastic processes. In addition practically the full polarizability of both the 2^3S and 2^1S states is included and a part of that of the ground state by using the 2^3P and 2^1P states in the close-coupling expansion. Cross sections for elastic scattering and for inelastic scattering from the ground state have been measured and we will attempt to compare our results with experimental information wherever possible. Cross sections involving only excited states have not been measured except in a few instances[12, 13] and our results thus represent predications of these cross sections which are expected to be reliable since all $n=2$ states are included in our expansion of the total wave function. Where comparisons can be made, agreement with experiment is satisfactory.

Our interest in these calculations has been mainly on resonant phenomena, and consequently the calculations were performed over a narrow energy range. The bulk of our calculations on processes involving ground-state excitation or elastic scattering is restricted to the range from the 2^3S threshold (19.82 eV above the helium ground state) to ~2.7 eV above it although we have extended our calculations (for s-wave scattering only) below this threshold to allow a comparison with other theoretical and experimental results. For processes involving only excited states of helium our calculations extend over a somewhat broader range of energies, from the 2^3S threshold to ~19 eV above it.

Apart from the purpose of providing realistic cross sections for low-energy impact of electrons on helium the work presented here serves another purpose. Our calculations indicate that there are a number of resonances in the vicinity of the $n=2$ thresholds of helium and that the apparent width of resonances which lie above the lowest-excitation threshold is of the same order of magnitude as the spacing of the $n=2$ helium excited states. There is to our knowledge no definitive theoretical treatment which accounts for the threshold behavior of cross sections when one or more broad resonances are interposed between the thresholds similar to that developed for two electron systems by Gailitis and Damburg.[14, 15] The treatment of Refs. 14 and 15 is not applicable to helium because the $n=2$ levels are not degenerate. We have attempted to discuss these resonances within the framework of existing theory, but feel that there is a need for a better understanding of resonances occurring above or between thresholds. It is hoped that our results will stimulate further theoretical work in this direction.

The outline of the remainder of the paper is as follows. Section 2 contains the theoretical development. The treatment is divided into two parts, namely (a) the discussion of the He bound-state wave functions used for the close-coupling expansion and (b) the derivation of the close-coupling equations for He electron scattering corresponding to expansion in the basis set discussed in (a). Section 3 is devoted to a description of what calculations were performed using the formalism described in Sec. 2. Section 4 presents detailed results of the cross sections obtained from these calculations and compares them with other theoretical and experimental work. The results are divided into subsections on ground state and metastable elastic scattering and on metastable and ground-state inelastic scattering, respectively. Section 5 is devoted to polarization of radiation resulting from impact excitation of the 2^3P and 2^1P states. Section 6 presents our analysis of the resonances. This treatment is somewhat separate from the rest of the paper since we have made no attempt to relate this analysis to the behavior of particular cross sections near resonance. Finally Sec. 7 is devoted to a summary and concluding remarks.

2. THEORY

A. The Atomic Wave Function

In this paper we describe calculations which have used two different approximations for the helium-atom eigenstate. We found that the results for some of the transitions were sensitive to the approximation. It is therefore necessary to discuss in some detail the motivation for our choices of atomic wave functions. The close-coupling expansion imposes three restrictions on this choice. First, all wave functions must be explicitly orthogonal otherwise it is not possible to separate unambiguously elastic scattering from excitation. Second, for reasons of numerical convenience the atomic wave functions must be in a form simple enough to make the close-coupling equations tractable. Finally, the wave functions must be asymptotically correct; i.e., at large distances (r_2) they must be of the form $U(r_1)\exp(-\epsilon_b^{1/2}r_2)$, where ϵ_b is the binding energy of the atomic state.

A set of atomic wave functions which satisfy all of these criteria has been generated as follows. We write the wave function for the $(1snl)^{2s+1}l$ state of helium in the form

$$\psi_{nls}^{m_l m_s}(1,2) = (8\pi)^{-\frac{1}{2}}[P_{\overline{1s}}(r_1)P_{nl}(r_2)Y_l^{m_l}(\hat{r}_2) + (-)^s P_{\overline{1s}}(r_2)P_{nl}(r_1)Y_l^{m_l}(\hat{r}_1)]\chi_s^{m_s}(1,2), \quad (1)$$

where $Y_l^{ml}(\hat{r})$ is the usual spherical harmonic, $P_{\overline{1s}}(r)$ is the $1s$ radial wave function of the helium positive ion, and $\chi_s^{m_s}(1,2)$ is the normalized two-particle spin function. We derive a radial

differential equation for the function $P_{nl}(r)$ from the variational principle

$$\delta \int \psi^*(1,2)(H_2 - E)\psi(1,2)d\tau_1 d\tau_2 = 0, \quad (2)$$

where the integral in Eq. (2) is taken over the space and spin coordinates of the two electrons; H_2 is the two-electron Hamiltonian and the variation is taken with respect to the functions $P_{nl}(r)$ subject to the usual boundary conditions. This equation was solved numerically. The solutions of the differential equation for different eigenvalues E_{nls} are automatically orthogonal. Further, for the excited states, the wave function is only slightly different from the Hartree-Fock solution and the eigenenergies are almost identical, since the inner electron orbital is not appreciably distorted by the outer electron. However, the ground-state eigenenergy is appreciably better than that for a closed-shell Hartree-Fock wave function. Using the trial function of equation (1) we obtain a binding energy of -2.8725 a. u. compared with the Hartree-Fock value of -2.8670 a. u. for the ground state.

An alternative set of atomic wave functions in analytic form were obtained from Eq. (2) by representing P_{nl} of Eq. (1) by the form

$$P_{nl}(r) = \sum_i c_i (2\xi_i)^{l_i + \frac{1}{2}} [(2l_i)!]^{-\frac{1}{2}} r^{l_i} \exp(-\xi_i r). \quad (3)$$

Wave functions of the form of Eq. (1) with this choice of $P_{nl}(r)$ for the $2\,^3S$, $2\,^3P$, and $2\,^1P$ states have been calculated previously[16] and have approximately the correct asymptotic behavior. For the $1s^2\,^1S$ state a single exponential was used in Eq. (3) and ξ varied to minimize the total energy. A wave function for $1s\,2s\,^1S$ was then obtained following the procedure of Marriott and Seaton[17] using their two exponentials for $P_{20}(r)$ and maintaining orthogonality to the $1s^2\,^1S$ state.[18] The coefficients c_i, ξ_i, and l_i for these wave functions, together with the eigenenergies, are given in Table I. Also shown are the eigenenergies for the numerical wave functions (E_{num}) and the experimental values (E_{exp}).

TABLE I. The coefficients defining the analytic helium-atom wave functions used in the scattering calculation. See Eq. (3) for a definition of the quantities.

State	c_i	ξ_i	l_i	E	E_{num}	E_{exp}
$1s^2\,^1S$	0.718 43	1.4907	1	−2.8649	−2.8725	−2.9037
$1s2s\,^3S$	0.266 39	1.57	1	−2.174	−2.1743	−2.175
	−1.061 92	0.61	2			
$1s2s\,^1S$	0.234 56	1.136	1	−2.1445	−2.1435	−2.1461
	−1.063 26	0.464	2			
$1s2p\,^3P$	1.0	0.55	2	−2.1305	−2.1313	−2.1333
$1s2p\,^1P$	1.0	0.485	2	−2.1225	−2.1225	−2.1239

B. The Scattering Equations

The total wave function with angular and spin quantum numbers L and S describing the scattering of an electron by a helium-atom state $n'l_1's_1'$ is written

$$\Psi^{LS}_{n_1' l_1' s_1' l_2'}(1,2,3) = 3^{-1/2} \sum_{nl_1s_1l_2} [\Psi^{LS}_{nl_1s_1l_2, n'l_1's_1'l_2'}(\tilde{12},3) + \Psi^{LS}_{nl_1s_1l_2, n_1'l_1's_1'l_2'}(\tilde{23},1) + \Psi^{LS}_{nl_1s_1l_2, n'l_1's_1'l_2'}(\tilde{31},2)],$$

where

$$\Psi^{LS}_{nl_1s_1l_2, n'l_1's_1'l_2'}(\tilde{12},3) = \sum_{\text{all } m} C_{l_1l_2}(LM_L; m_{l_1} m_{l_2}) C_{s_1\frac{1}{2}}(SM_S; m_{s_1} m_{s_2}) \times \psi_{nl_1s_1}{}^{m_{l_1} m_{s_1}}(1,2) F^{LS}_{nl_1s_1l_2, n'l_1's_1'l_2'}(r_3) Y_{l_2}{}^{m_{l_2}}(r_3) \chi_{\frac{1}{2}}{}^{m_{s_2}}. \quad (4)$$

We now derive coupled integro-differential equations for the functions $F(r)$, which describe the motion of the scattered electron. Writing the asymptotic form of the function $F(r)$ as

$$F_{ij}{}^{LS}(r) \sim k_i^{-\frac{1}{2}} [\delta_{ij} \sin(k_i r - \tfrac{1}{2} l_i \pi) + R_{ij}{}^{LS} \cos(k_i r - \tfrac{1}{2} l_i \pi)], \quad \text{as } r \to \infty, \quad (5)$$

where i corresponds to $nl_1s_1l_2$ and j corresponds to $n'l_1's_1'l_2'$, then the Kohn variational principle can be written

$$\delta[\int \Psi_i{}^{LS\dagger}(1,2,3)(H_3 - E)\Psi_j{}^{LS}(1,2,3)d\tau_1 d\tau_2 d\tau_3 - \tfrac{1}{2} R_{ij}{}^{LS}] = 0. \quad (6)$$

Here H_3 is the three electron Hamiltonian and the variation is taken with respect to the functions F subject to the boundary conditions defined by Eq. (5).

In the reduction of Eq. (6) we make one approximation. The exchange term which is proportional to

$$\sum_{kl}\int \Psi_{ki}^{LS\dagger}(1\tilde{2},3)(H_3-E)\Psi_{lj}^{LS}(1\tilde{3},2)d\tau_1 d\tau_2 d\tau_3 \tag{7}$$

is replaced by

$$\sum_{kl}\int \Psi_{ki}^{LS\dagger}(1\tilde{2},3)(\tfrac{1}{2}\nabla_1^2+2/r_1+1/r_{23}-E+E_k+E_l)\Psi_{lj}^{LS}(1\tilde{3},2)d\tau_1 d\tau_2 d\tau_3, \tag{8}$$

where E_k and E_l are the appropriate eigenenergies of the helium atom determined from Eq. (2). Equation (8) only follows rigorously from Eq. (7) if the helium wave function given by Eq. (1) is an exact solution of the two electron Schrödinger equation rather than a solution of the variational principle given by Eq. (2). This approximation introduces an error of unknown magnitude into the calculation, and also, more importantly, means that our final solution does not satisfy exactly the Kohn variational principle. This error, since it is in the short-range exchange terms, can be expected to be most important for the low partial waves, and we argue in later sections that it severely limits the accuracy of our S-wave solutions.

The reduction of Eq. (6) now follows in a straightforward manner, and we obtain the following coupled integro-differential equations for the functions $F(r)$:

$$\left(\frac{d^2}{dr^2}-\frac{l_2(l_2+1)}{r^2}+\frac{4}{r}+k_i^2\right)F_{il}(r)=\sum_j[V_{ij}(r)F_{jl}(r)+\int_0^\infty K_{ij}(r,r')F_{jl}^{LS}(r')dr'], \tag{9}$$

where $k_i^2=2(E-E_{nl_1s_1})$;

$$\begin{aligned}
V_{ij}(r)=2\delta_{s_1s_1'}\sum_\lambda[&y_0(P_{\overline{1s}}P_{\overline{1s}};r)\Delta(P_{nl_1}P_{n'l_1'})\delta_{l_1l_1'}\delta_{l_2l_2'}\delta_{\lambda 0}+f_\lambda(l_1l_2l_1'l_2';L)\Delta(P_{\overline{1s}}P_{\overline{1s}})y_\lambda(P_{nl_1}P_{n'l_1'};r)\\
&+(-)^{s_1}\left(\frac{2l_2+1}{(2L+1)(2l_1+1)}\right)^{\frac{1}{2}}C_{l_1l_2}(L\,0;00)\Delta(P_{\overline{1s}}P_{n'l_1'})y_{l_1}(P_{nl_1}P_{\overline{1s}};r)\delta_{\lambda l_1}\delta_{l_1'0}\delta_{l_2'L}\\
&+(-)^{s_1}\left(\frac{2l_2'+1}{(2L+1)(2l_1'+1)}\right)^{\frac{1}{2}}C_{l_1'l_2'}(L\,0;00)\Delta(P_{nl_1}P_{\overline{1s}})y_{l_1'}(P_{\overline{1s}}P_{nl_1'};r)\delta_{\lambda l_1'}\delta_{l_10}\delta_{l_2L}];
\end{aligned}$$

$$\begin{aligned}
\int_0^\infty K_{ij}(r,r')F_{jl}^{LS}(r')dr'=-2b_{s_1s_1'}\sum_\lambda\Big\{&g_\lambda(l_1l_2l_1'l_2';L)y_\lambda(P_{nl_1}F;r)P_{n'l_1'}(r)\\
&-(E-E_{nl_1s_1}-E_{n'l_1's_1'}-2)\Delta(P_{nl_1}F)P_{n'l_1'}(r)\delta_{\lambda 0}\delta_{l_1l_2'}\delta_{l_2l_1'}\\
&+(-)^{s_1}\delta_{l_10}\delta_{l_2L}\Big[\left(\frac{2l_1'+1}{(2l_2'+1)(2L+1)}\right)^{\frac{1}{2}}C_{l_1'l_2'}(L\,0;00)\Delta(P_{nl_1}P_{\overline{1s}})y_{l_2'}(P_{\overline{1s}}F;r)P_{n'l_1'}(r)\\
&-(E-E_{nl_1s_1}-E_{n'l_1's_1'}-2)\Delta(P_{nl_1}P_{\overline{1s}})\Delta(P_{\overline{1s}}F)P_{n'l_1'}(r)\delta_{l_1'L}\delta_{l_2'0}\Big]\\
&+(-)^{s_1'}\delta_{l_1'0}\delta_{l_2'L}\Big[\left(\frac{2l_1+1}{(2l_2+1)(2L+1)}\right)^{\frac{1}{2}}C_{l_1l_2}(L\,0;00)\Delta(P_{\overline{1s}}P_{n'l_1'})y_{l_2}(P_{nl_1}F;r)P_{\overline{1s}}(r)\\
&-(E-E_{nl_1s_1}-E_{n'l_1's_1'}-2)\Delta(P_{\overline{1s}}P_{n'l_1'})\Delta(P_{nl_1}F)P_{\overline{1s}}(r)\delta_{l_1L}\delta_{l_20}\Big]\\
&+(-)^{s_1+s_1'}\delta_{l_2l_2'}\delta_{l_1l_1'}\Big[\frac{1}{2l_2+1}\Delta(P_{nl_1}P_{n'l_1'})y_{l_2}(P_{\overline{1s}}F;r)P_{\overline{1s}}(r)\\
&-(E-E_{nl_1s_1}-E_{n'l_1's_1'})\Delta(P_{nl_1}P_{n'l_1'})-\tfrac{1}{2}\Delta(P_{nl_1}D_LP_{n'l_1'})\Delta(P_{\overline{1s}}F)P_{\overline{1s}}(r)\delta_{l_1L}\delta_{l_20}\Big]\Big\}.
\end{aligned} \tag{10}$$

The quantities Δ, y_λ, f_λ, and g_λ used in Eq. (10) have been defined by Percival and Seaton,[19] and we have also defined

$$D_L=d^2/dr^2-L(L+1)/r^2+4/r$$

and $b_{s_1s_1'}=(\tfrac{1}{2}-s_1)\delta_{s_1s_1'}-\tfrac{1}{2}(3)^{1/2}(1-\delta_{s_1s_1'})$.

The numerical solution of the Eq. (9) follows standard procedures. We replace the exchange terms by additional coupled differential equations, following Marriott[20] and solve the resultant set of coupled differential equations by a method which involves outward integration from the origin and inward integration from the asymptotic region. The subsequent matching, as discussed by Burke and Smith[21] at an intermediate value of the radius, yields the R matrix defined by Eq. (5) for given values of L, S, and E. From the R matrix the S (scattering) and T (transmission) matrices are obtained by the well-known relations:

$$S = (1+iR)/(1-iR), \quad T = S-1. \tag{11}$$

Total cross sections for transitions between any two states (p, q) of the close-coupling expansion are obtained via the relation

$$\sigma_{pq} = \frac{1}{k_p^2} \sum_{L,S,l_1',l_2'} \frac{1}{2} \frac{(2L+1)(2S+1)}{(2l_1'+1)(2l_2'+1)} |T_{pq}|^2 . \tag{12}$$

3. DESCRIPTION OF CALCULATIONS

Using the formalism described in the preceding section, we have obtained solutions of the coupled equations for e-He for various values of L, S, and E. These solutions provide cross sections for all elastic and inelastic processes between the 5 states included in our expansion.

Since the coupling between the ground state and the four excited states is weak, it is not necessary to include the ground-state channel in the calculation if cross sections involving only the excited states are desired. However, since the resonance structure in the $L=0$, 1, and 2 partial waves has a marked effect on all cross sections it is necessary that all four coupled $n=2$ states be included to obtain reasonable results. Further, it is necessary that the bound-state wave functions used in the eigenfunction expansion be accurate enough to give the correct resonance structure.

For processes involving excitation of the ground state in the neighborhood of the excitation thresholds of the $n=2$ states, all five states in the eigenfunction expansion must be included. Furthermore, these calculations provide a useful check on how well we have obtained the resonance structure in our eigenfunction expansion because direct comparison with experimental evidence is possible.

The calculations on which the major portion of the results reported in this paper are based can be conveniently grouped into two sets A and B, as described below.

Set A: This refers to calculations including all 5 states in the eigenfunction expansion for $L=0$, 1, 2; $S=\frac{1}{2}$ and covering the energy range ~1.3–1.6 Ry above the ground state. In these calculations the numerical bound-state wave functions described in Sec. 2.1 were used in the eigenfunction expansion and the excitation thresholds were assumed to be given by the calculated energies of these states.

Set B: This refers to calculations including only the four $n=2$ states in the eigenfunction expansion. Calculations were performed for $S=\frac{1}{2}$, $\frac{3}{2}$, and for various values of L depending on the energy in the energy range of 0–1.2 Ry above the $2\,^3S$ threshold. In these calculations the analytic wave functions discussed in Sec. 2.1 were used in the eigenfunction expansion, and the excitation thresholds were assumed to be at their experimentally determined positions.

We performed the 4 state and 5 state calculations using different wave functions and excitation thresholds partly to assess the effects of such variations on our results, but mainly because the analytic functions were the best available for our initial calculations. Since the calculations of Set B do not contain the ground-state channel, the effects of using different wave functions and excitation thresholds in Sets A and B can only be accessed by their effect on the cross sections involving the four $n=2$ states. The major difference between the two calculations was a shift in energy of the positions of resonances lying immediately above the $2\,^3S$ threshold. At the highest energy at which Set A calculations were made (0.2 Ry above the $2\,^3S$ threshold) both calculations produced cross sections (for $L=0$, 1, and 2; $S=\frac{1}{2}$) which generally agreed to within 10%. Deviations are interpreted to be due to shifts in the resonance positions at lower energies (which in turn leads to marked discrepancies between the two calculations for given L and S at energies near the resonances) rather than to differences in the atomic wave functions used for the two calculations.

The results of these calculations take the form of R matrices as defined by Eq. (5) and of a matrix of cross sections for all energetically allowed processes computed according to Eq. (12) for each value E. In reporting the results of these calculations we have adopted the policy in the next three sections of presenting curves which illustrate what we have been able to abstract from the calculated results. For more detailed comparison with future experiments or for those who may wish to abstract further information from these calculations the complete results of

Sets A and B will be made available by the authors on request.

4. CROSS SECTIONS

A. Elastic Scattering from the Ground State

Detailed results for elastic scattering from the ground state are available from the Set A computations only in the energy range of ~19.8–22.5 eV. However, since a resonance has been reported at 0.45 eV[22] and there have been several recent attempts at definitive calculations for ground-state elastic scattering[6,23,24] we have extended the range of our $L=0$ results below the ^3S threshold. In Fig. 1 we show the $L=0$ phase shift (δ_0) from this calculation together with two previous estimates. Our phase shift is in good agreement with both calculations at the lowest energy in our calculations ($k=0.1$, $\delta_0=3.0147$) and lies somewhat below the others in the range $k=0.1-0.7$ and there is no evidence of a resonance in this region. If it exists in our approximation it must be at least an order of magnitude narrower than our tabulation interval which was 0.01 Ry. Above $k=0.80$ the phase shift tends to flatten out as the resonance at $k\sim1.167$ (which corresponds to the 19.3-eV resonance in elastic scattering) is approached. At higher k values the S-wave phase shift is not uniquely defined in our calculation since other channels are open. For comparison purposes we have defined an effective S-wave phase shift from our $L=0$ elastic scattering results (σ_0) via the relation

$$|\delta_{\text{eff}}|\,(\text{mod}\,\pi)=\sin^{-1}[k\sigma_0^{1/2}/2]\,.$$

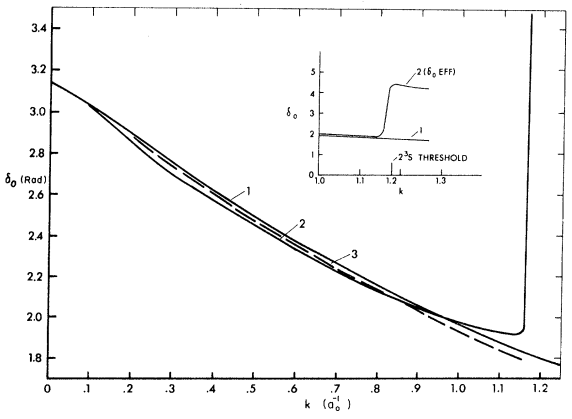

FIG. 1. The $L=0$ phase shift (δ_0) versus k. (1) Reference 23; (2) this paper; and (3) Ref. 24. The inset shows the effective phase shift δ_{eff} as defined in the text in the neighborhood of the excitation threshold.

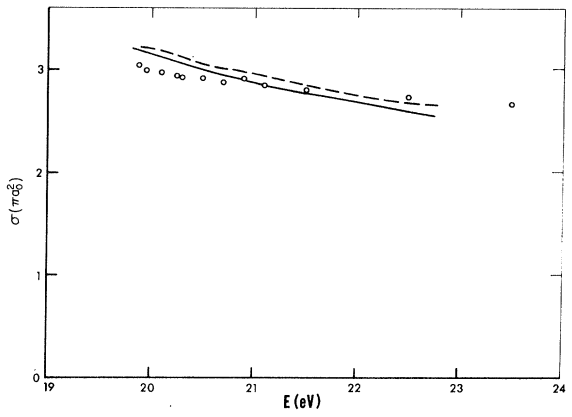

FIG. 2. Total scattering from the 1^2S state. Solid line: elastic scattering; dashed line: total scattering; ○, experimental points from Ref. 25.

The extension of δ_0 via δ_{eff} through the resonance is shown in the inset of Fig. 1. Above the 2^3S threshold $|\delta_{\text{eff}}|$ is smaller (~1.1 mod π) and decreases faster with increasing energy than predicted by previous calculations.

The total and elastic cross sections (based on our $L=0$, 1, and 2 results) are compared in Fig. 2 with the measurement of Golden and Bandel[25] in the 19.8- to 23.5-eV region. Previous calculations predict larger cross sections in the region above 20 eV, a direct consequence of their $L=0$ phase shifts being closer to $\frac{1}{2}\pi$ than our $|\delta_{\text{eff}}|$.

For comparison with experiment at lower energies we have used the data of Ref. 6 to estimate the P and D wave contributions to the cross section and our phase shifts for the S wave contribution. The results are compared with the experiment of Ref. 25 in Fig. 3. We see that our calcu-

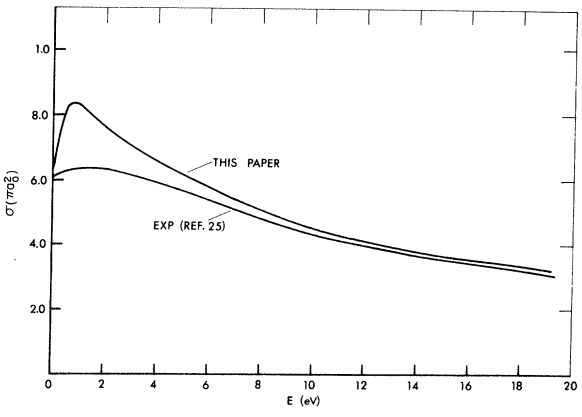

FIG. 3. Elastic scattering from zero to 19 eV based on the $L=0$ results of this paper and the $L=1$ and 2 results of Ref. 23.

lation is in good agreement with experiment down to energies of ~ 10 eV. Below this energy our calculation predicts cross sections larger than observed, a direct consequence of the close-coupling calculation including only 35% of the full polarizability since only the $n=2$ states are included in the calculation.

B. Elastic Scattering from $n = 2$ States

The calculations of Sets A and B provide two estimates of the $L=0$, 1, and 2 partial-wave contributions to these cross sections (and all other cross sections between $n=2$ states) in the energy range 0–0.2 Ry above the $2\,^3S$ threshold. To obtain the best estimate of these cross sections we have combined the $L=0$, 1, and 2 doublet contributions of Set A with the $L>2$ doublet contributions and quartet contributions for all L values from Set B in this energy range. The results from Set B for all L values were used for higher energies. The rationale for this procedure is that for $L=2$ the two sets of calculations gave results in close agreement with each other, whereas for $L=0$, and 1, deviations occurred since Set A gives better results for the resonance positions in the region where new channels are opening up. The comparison of the Set A calculations with experiment for ground-state excitation processes (to be discussed in Sec. 4D) indicate that these calculations correctly predict the positions of resonances and should provide good estimates for all transitions between $n=2$ states. The Set B results should provide good estimates for higher L values and at higher energies.

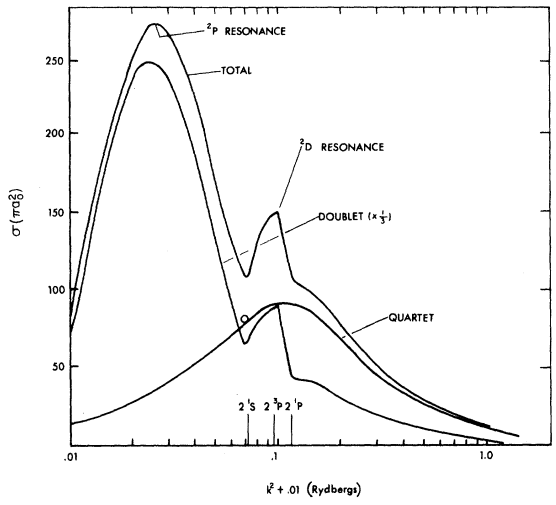

FIG. 4. Elastic scattering from the $2\,^3S$ state. The points shown are Marriott's (Ref. 9) estimates of the quartet scattering in the $1\,^1S$–$2\,^3S$–$2\,^1S$ approximation. The figure is plotted on a semilog scale versus $k^2+0.01$ (Rydbergs) to emphasize the resonant structure in the energy range above the $2\,^3S$ threshold.

In Fig. 4 the $2\,^3S$ elastic cross section is plotted along with the individual doublet and quartet contributions and the results of a previous calculation.[9] The prominent features are the large values of the cross sections at $k^2\sim 0.02$, $k^2\sim 0.09$ due to the ^2P and ^2D resonances in the atom-plus-electron system. Note that no ^4P resonance structure is present in the quartet state. The ^4P analog of the state responsible for the ^2P resonance at ~ 0.03 Ry above the $2\,^3S$ threshold lies at 0.080 eV below threshold[26] and thus produces no resonance in the $2\,^3S$ elastic cross section. No resonant structure is apparent in other partial waves. The lack of resonances probably accounts for the good agreement between our (2 state) and Mariott's[9] (1 state) $2\,^3S$ elastic scattering results for quartet scattering. His values at higher energies are understandably lower than ours since only the first few partial waves are included in his calculation (our calculation includes partial waves up to $L=31$ for $k^2=1.2$ Ry). The doublet contribution in Marriott's work (not shown) is substantially lower than ours since the resonances are not reproduced by his calculation. Two other calculations of elastic scattering from $2\,^3S$ taking into account polarization effects have been made.[27,28] The calculations of Husain *et al.*[27] make no attempt to separate doublet and quartet contributions to the cross section and ignore exchange effects. Their work predicts cross sections substantially larger than those reported here. Sklarew and Callaway[28] have performed calculations of $2\,^3S$ elastic scattering using adiabatic and extended polarization approximations and including exchange and spin effects. Their calculations do not predict correctly the positions of the ^2P and ^2D resonances in the doublet cross section. However, their calculations in the extended polarization approximation are in reasonably good agreement with ours in the region 0.1–1.0 Ry above the ^3S threshold, their cross sections being 30–40% lower than our values. This is consistent with the statement made in Ref. 28 that exchange, polarization, and distortion are all important effects (all are implicitly included in the close-coupling calculations) for near-threshold elastic scattering from excited states.

The elastic scattering cross section from the $2\,^1S$ state is shown in Fig. 5. The $L=0$ partial wave appears to resonate near threshold (we obtain a value of the $L=0$ cross section of $1430\pi a_0^2$ at 0.0014 Ry above the threshold). The $L=0$, 1, 2, and 3 partial-wave contributions to this cross section in the resonance region are shown in the figure.

Cross sections for elastic scattering in doublet

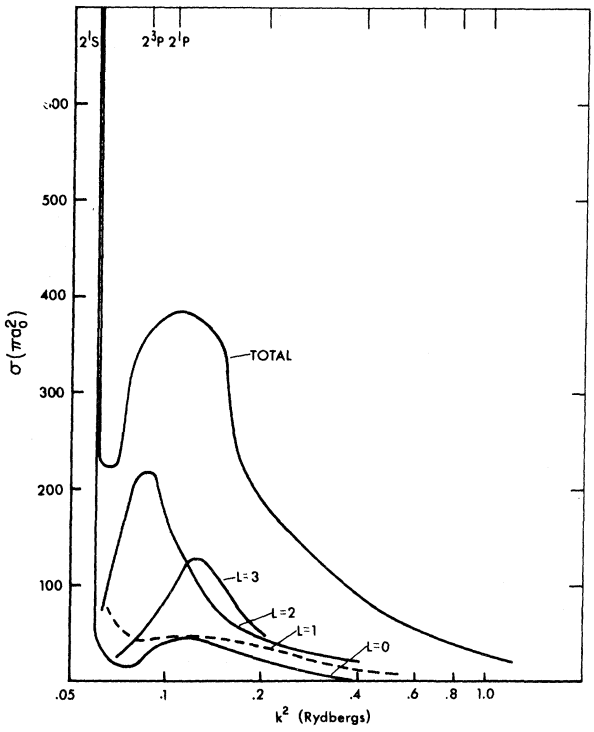

FIG. 5. Elastic scattering from the $2\,^1S$ state. k^2 (Rydbergs) is the energy above the $2\,^3S$ threshold.

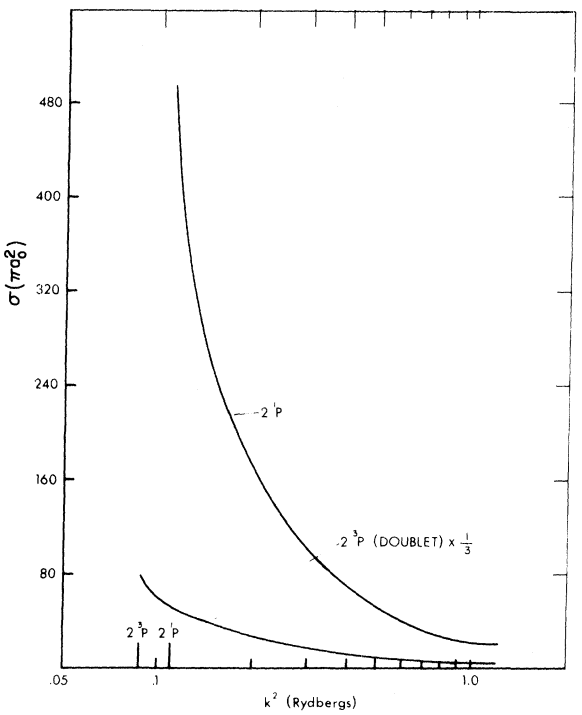

FIG. 6. Elastic scattering from $2\,^3P$ and $2\,^1P$ states. k^2 (Rydbergs) is the energy above the $2\,^3S$ threshold.

states from the $2\,^3P$ and $2\,^1P$ states are shown in Fig. 6. These cross sections are large near threshold and decrease with increasing energy. Unfortunately the quartet scattering contribution for ^3P scattering was not evaluated and thus we can make no estimate of the total cross section.

C. Excitation of $n = 2$ States

Figure 7 shows the cross sections for excitation of $2\,^3S$ to $2\,^1S$, $2\,^3P$ and $2\,^1P$ states and Fig. 8 displays the remaining "upward" transitions from $2\,^1S$ and $2\,^3P$ states.[29] These curves display the complex resonant structure inherent in our calculation. While the peaks in various cross sections at the lower energies are due to a single resonance (e.g., the peaks at $k^2 = 0.08$ in $2\,^3S$-$2\,^1S$ excitation and at $k^2 \sim 0.1$ in $2\,^3S \rightarrow 2\,^1S$, $2\,^3P$ and $2\,^1S$-$2\,^3P$ correspond to the ^2P and ^2D resonances) the large values of the $2\,^3S$-$2\,^3P$ quartet contribution and of the $2\,^1S$-$2\,^1P$ cross section are not caused by single resonance but rather to the sum of all the partial-wave contributions for $L \geq 3$. Also note that the cross sections for these processes vary over approximately two orders of magnitude. The asymptotic form of the Born approximation cross section at high incident energies for $2\,^1S$-$2\,^1P$ transitions will be of the form[30]

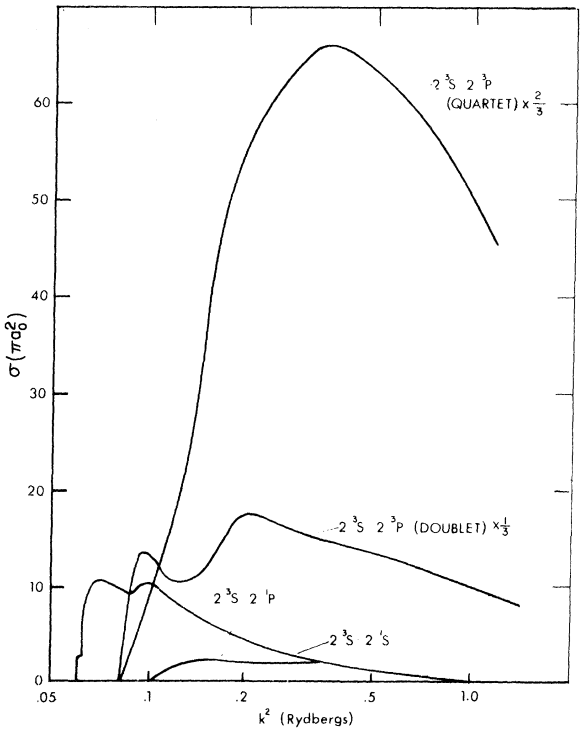

FIG. 7. Inelastic scattering from the $2\,^3S$ state. k^2 (Rydbergs) is the energy above the $2\,^3S$ threshold.

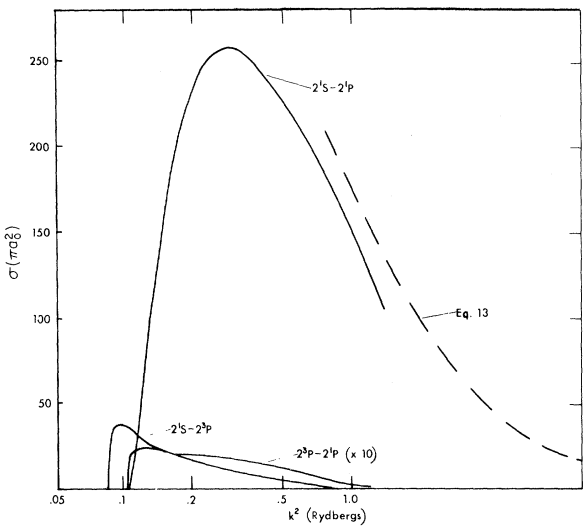

FIG. 8. Inelastic scattering from $2\,^1S$ and $2\,^3P$ states. k^2 (Rydbergs) is the energy above the $2\,^3S$ threshold. The dashed curve is the asymptotic Born approximation as given by Eq. (13).

$$\sigma_{\text{Born}}(2\,^1S\text{-}2\,^1P) = (4/k^2)[A\ln(k^2) + B + C/k^2](\pi a_0^2). \tag{13}$$

The constants A, B, and C depend only on the optical oscillator strength $2\,^1S\text{-}2\,^1P$ and the generalized oscillator strength $f(Q)$ (Q is the momentum transfer in atomic units) and $[df(Q)/dQ]$ for $Q=0$. These constants have been evaluated by Kim[31] and are $A=8.50$, $B=41.97$, and $C=-0.0153$. A plot of Eq. (13) using these constants is shown in Fig. 8. A comparison with our calculation indicates surprisingly that the asymptotic form given by Eq. (13) is a relative good approximation even for energies as low as 1 Ry above threshold.

The cross sections for the inverse ("superelastic") processes to those shown in Figs. 6 and 7 were also obtained in our calculation. Since these cross sections can be obtained from the cross sections shown in Figs. 6 and 7 by applying the detailed balance relation[32] we do not present figures for these cross sections. Because of resonant effects these cross sections attain extremely large values near threshold. An example of this is shown in Fig. 9 which compares our cross section for the process $2\,^1S \rightarrow 2\,^3S$ with a previous measurement.[13]

Neynaber *et al.*[12] have measured the cross section for removing $2\,^3S$ states from a metastable beam by electron impact at 5 energies between 0.87 and 8.25 eV. In Fig. 10 their results are compared with the sum of all cross sections which we have calculated which have $2\,^3S$ as an initial state in this energy range. Our results lie within the experimental uncertainties for only one point (at $E=1.4$ eV) in Fig. 10. At the two higher points the disagreement is not serious since excitation to higher states and ionization which are not included in our calculations probably account for the difference between calculated and measured values. The large excess in measured over-calculated cross sections at the lower energies is more serious since our calculation should include all processes.

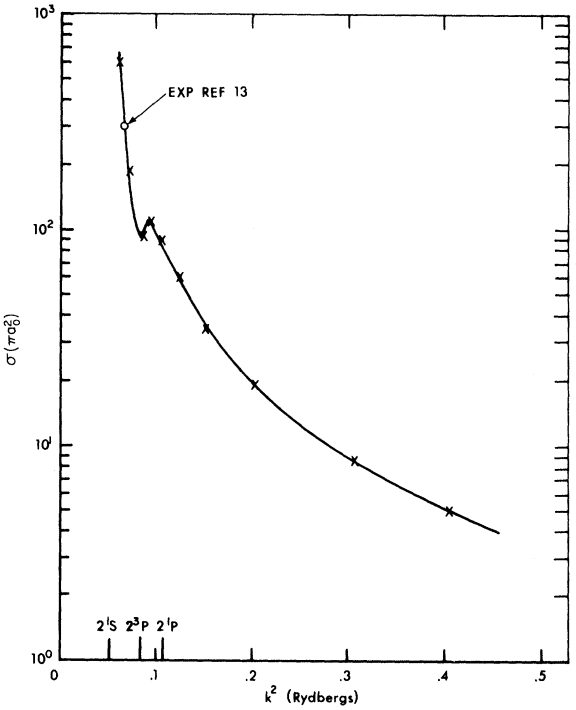

FIG. 9. The $2\,^1S \rightarrow 2\,^3S$ superelastic cross section. The experimental point is from Ref. 13. Crosses indicate energies at which calculations were carried out.

D. Excitation from the Ground State

The cross sections for excitation of $n=2$ states from the $^1S_0$ ground state are difficult to calculate since they are small owing to the weak coupling between the ground-state channel and the four or six $n=2$ channels. Thus these cross sections are typically several orders of magnitude smaller than the cross sections discussed in the previous sections. Also the cross sections for excitation in the vicinity of the $n=2$ thresholds proceeds primarily by excitation to resonant He^- states followed by decay into one or the other of the various open channels. Our calculations have been successful in predicting the positions of these resonances. Deviations from experimentally measured cross sections are apparent for

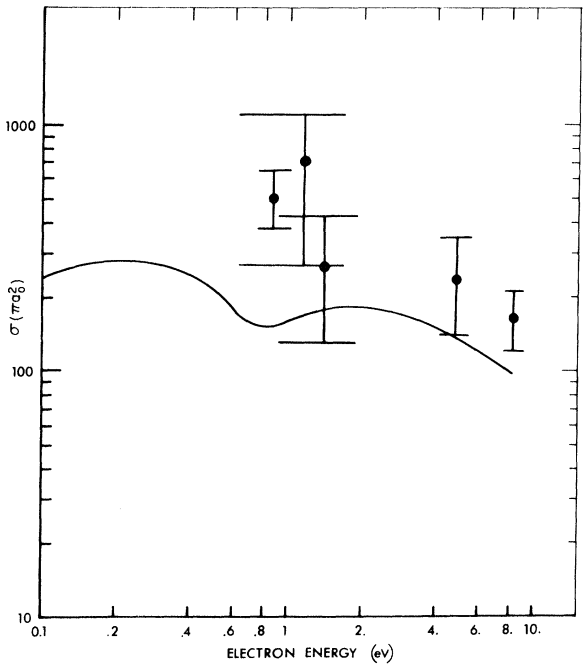

FIG. 10. Total cross sections for scattering from the $2\,^3S$ state. The error bars on the experimental points (Ref. 12) indicate the estimated width of the electron beams used. No attempt has been made in the theoretical curve to plot the details of the resonant structure.

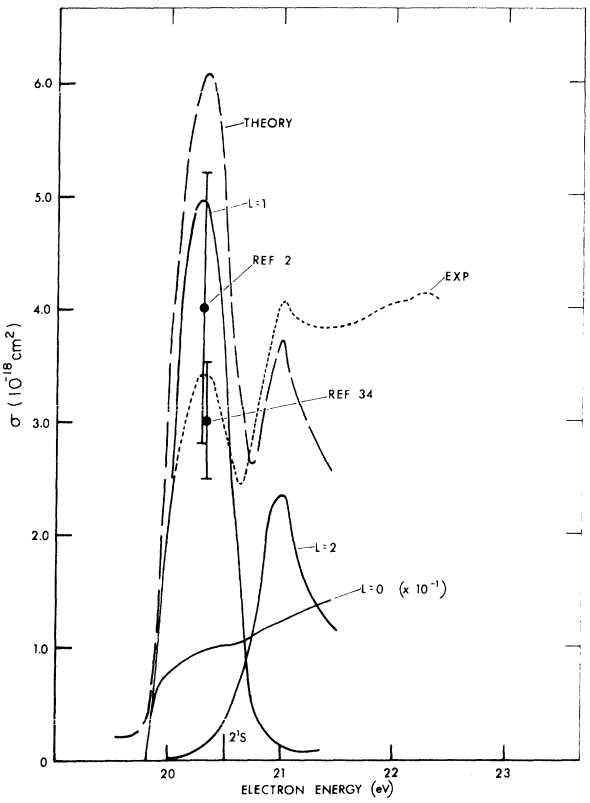

FIG. 11. The calculated $2\,^3S$ cross section compared with the experimentally measured total metastable production. The points shown are the absolute values at the first peak from Refs. 2 and 34. The $L=0$ component is scaled by a factor of 10^{-1}.

$L=0$ and $L=1$ angular momentum states.

We consider first $2\,^3S$ excitation since this cross section provides a direct comparison with experimental results. Figure 11 shows the results of our Set A calculations for $L=0$, 1, and 2 partial waves compared with a recent measurement[33] of total metastable production. Earlier measurements of this cross section[2] with somewhat poorer energy resolution produced curves of similar shape. The absolute value of the first peak has been measured by two investigators[2,34] and their results, and estimated uncertainties are also shown. The relative cross section of Ref. 33 has been arbitrarily normalized to 3.4×10^{-18} cm^2 at the first peak.

The data presented in Fig. 11 indicate that our $L=1$ and $L=2$ partial cross sections are approximately correct in both shape and absolute value and that the first two peaks in the metastable production curve are due predominantly to ^2P and ^2D resonances in the $2\,^3S$ excitation cross section. This figure also shows that our $L=0$ component is too large by approximately an order of magnitude. We attribute the large calculated value of the $L=0$ component to a large coupling being introduced between the ground-state channel and the excited-state channels, probably by the approximation of Eq. (8). We obtained further evidence of this by extending the Set A calculations for $L=0$ below the $2\,^3S$ threshold. This extension produced an elastic $L=0$ resonance at 19.33 eV with a width of 0.039 eV as reported previously [Ref. 10(a)]. The position of the resonance agrees well with experimental results, but the width is certainly too large[35] by at least a factor of 2. If the error in the coupling is independent of energy we could simply scale our computed results by the ratio of expected to calculated widths of the 19.3-eV resonance as was done in Ref. 10(a). The same procedure is suggested by two channel effective range theory [Ref. 5(a)]. This procedure is expected to be valid at best only in the immediate vicinity of the $2\,^3S$ threshold.

The assignment of the first two peaks in the total metastable production curve to ^2P and ^2D resonances in the $2\,^3S$ excitation cross section has been verified by Ehrhardt *et al.*[36,37] who measured the angular distribution of electrons which have excited the $2\,^3S$ state.

The angular distribution can be obtained from our calculation. In terms of the T matrix [Eq. (11)]

the angular distribution for $1\,^1S - 2\,^3S$ scattering is

$$\sigma(\theta, k_2) = (4k_1^2)^{-1} \left| \sum_L (2L+1) \times T_{12}^{(L)}(k_2) P_L(\cos\theta) \right|^2 , \qquad (14)$$

where $T_{12}^L(k_2)$ is the T-matrix element corresponding to $1\,^1S_0 - 2\,^3S$ scattering. As in Ref. 10(a) we scale the $T_{12}^0(k_2)$ matrix elements by $1/\sqrt{10}$ to obtain an approximation to the true $L=0$ contribution to the differential cross section. This assumes that the relative phase as well as the energy dependence of $T_{12}^0(k_2)$ is not affected by the errors in our calculation. The angular distribution for $2\,^3S$ excitation based on our Set A calculations is shown in Fig. 12 along with the experimental results of Ref. 36. Several things are apparent from the comparison of the theoretical and experimental curves. First the general shape of the theoretical and experimental curves at 30°, 60°, and 90° is roughly the same. This indicates that the relative magnitude of the matrix elements $T_{12}^0(k_2)$ and their phases are approximately correct. A detailed analysis of the experimental results[36] shows that the peaks at ~20.4 and 21 eV are predominantly of ^2P and ^2D character in agreement with our calculations.

The peak immediately above the $2\,^3S$ threshold which has been detected in forward scattering[38] and becomes more prominent as the scattering angle is increased is still not completely understood. Ehrhardt *et al.*[37] have analyzed their experimental data in terms of elastic and inelastic phase shifts near the $2\,^3S$ threshold, and on this basis have attempted to separate the $L=0$, 1, and 2 wave contributions to their experimental cross sections. Their results indicate that the $L=1$ and $L=2$ partial-wave contributions near threshold are similar to those shown in Fig. 11 but that the $L=0$ contribution is larger than we calculate near threshold and drops rather than rises as energy increases. We verify from our solution that the mixing parameter defined in Ref. 36 is essentially constant in energy which implies therefore that our $2\,^3S$ eigenphase drops slower with energy than it should. This is consistent with our $1\,^1S - 2\,^3S$ coupling being too strong and thus causing too much repulsion between the two eigenphases. A better understanding of the near threshold behavior will require an improved calculation of the $L=0$ partial-wave contribution.

From the measured angular distributions of Fig. 12 it would appear that the peak immediately above threshold should be detectable in measurement of the total cross section of Ref. 31. To investigate this apparent discrepancy we have repeated the calculation of the angular distribution for the $2\,^3S$ cross section but have scaled the $T_{12}^0(k_2)$ matrix elements of Eq. (14) by $\frac{1}{2}$ rather than $1/\sqrt{10}$ and have extended the calculated angular distributions to angles greater than 90°.[39] This calculation, shown in Fig. 13 produces angular distributions for angles to 90° which are in better agreement with the measurements of Ref. 34 than those shown in Fig. 12. It also indicates that failure to observe the peak right above threshold in the total cross section is that due to absence of the peak in the backward direction. This inter-

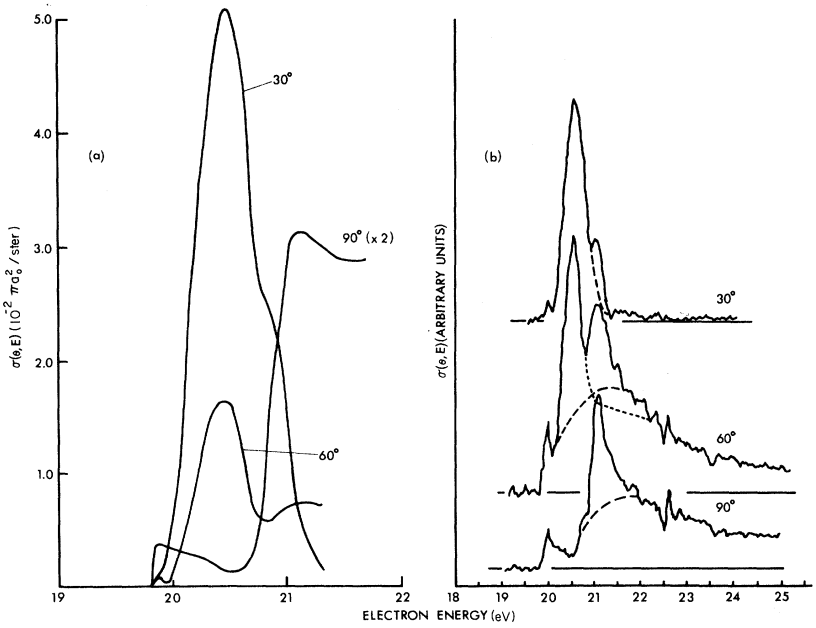

FIG. 12. Spectra for excitation of $2\,^3S$ at 30°, 60°, and 90°. (a) This paper scaling T_{12}^0 of Eq. (14) by $1/\sqrt{10}$; (b) Ref. 36.

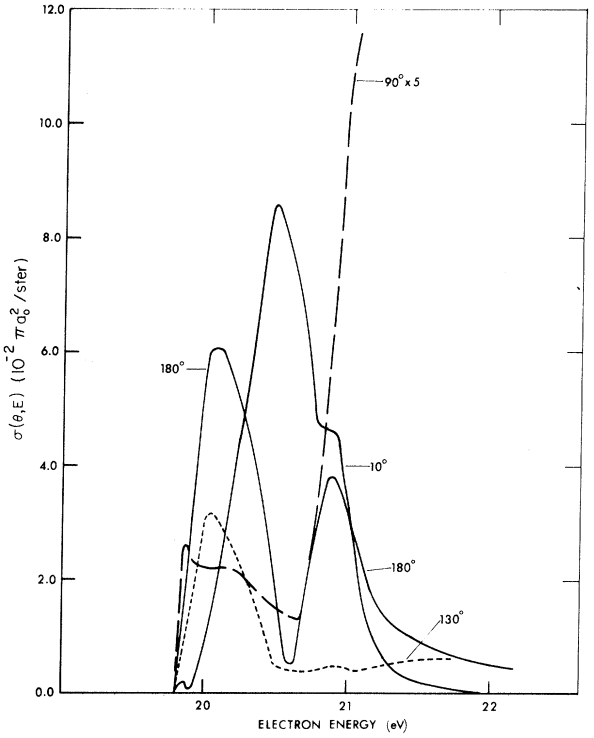

FIG. 13. Spectra for excitation of $2\,^3S$ at 10°, 90°, 130°, and 180° scaling $T_{12}{}^0$ of Eq. (14) by $\frac{1}{2}$.

pretation is consistent with the partial-wave contributions shown in Fig. 11. Scaling $T_{12}{}^0(k_2)$ by $\frac{1}{10}$ rather than $1/\sqrt{10}$ is equivalent to scaling the $L=0$ component in Fig. 11 by 0.25 rather than 10^{-1}. However, even increasing the $L=0$ component shown in Fig. 11 by a factor of 4 would not produce a peak close to threshold in the total cross section.

In spite of the uncertainties in the $L=0$ contribution to differential and total cross sections, our calculations together with the experimental results of Refs. 36 and 37 definitely establish the important role played by the ^2P and ^2D resonances in the near threshold region. The major discrepancy between calculated and measured angular distributions is that the calculated results are obviously incorrect at energies greater than 21.2 eV (which is not surprising since only $L=0$, 1, and 2 partial waves have been included in the calculation and our estimate of the $L=0$ component will be poorer the further we go from threshold).

The scaling procedure used for the $L=0$ component of the $2\,^3S$ excitation cross section is expected to be poorer for the $2\,^1S$, $2\,^3P$, and $2\,^1P$ cross sections. Nevertheless, we have applied it to these cross sections in order to obtain estimates of their size and for comparison with existing experimental data. In Fig. 14 we show spectra at 10°, 30°, and 90° based on our calculations for $2\,^1S$ excitation and measured spectra at these angles from Ref. 37. Ehrhardt *et al.*[37] ascribe the first peak in this cross section which becomes prominent at 90° to a ^2S resonance. Our calculations indicate the presence of this resonance but it appears prominently only in elastic $2\,^1S$ scattering. As in the case of $2\,^3S$ excitation our scaling of the $L=0$ wave partial-wave contribution probably gives an underestimate near threshold. Further evidence that we are underestimating the $2\,^1S$ cross section is provided by Chamberlain's results.[38] The ratio of the peak values of $2\,^3S$ to $2\,^1S$ in forward scattering is ~8 from his measurements whereas our calculated value is ~15. How this factor of 2 discrepancy in the forward direction affects our estimate of the total $2\,^1S$ cross section is uncertain.

In Fig. 15 we show total cross sections for $2\,^1S$, $2\,^3P$, and $2\,^1P$ excitation. We believe the P- and D-wave contributions of these cross sections to be substantially correct, although the recent results of Ref. 37 indicate that the D wave may be more dominant at 22 eV in $2\,^1S$ excitation than we calculate. The $2\,^1S$ and $2\,^3P$ cross sections are expected to be reasonable estimates since the

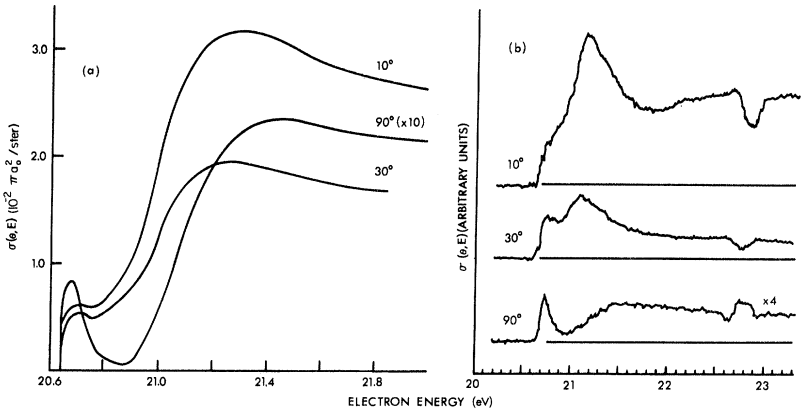

FIG. 14. Spectra for excitation of $2\,^1S$ at 10°, 30°, and 90°. (a) This paper scaling $T_{13}{}^0$ of Eq. (14) by $\sqrt{10}$; (b) Ref. 36.

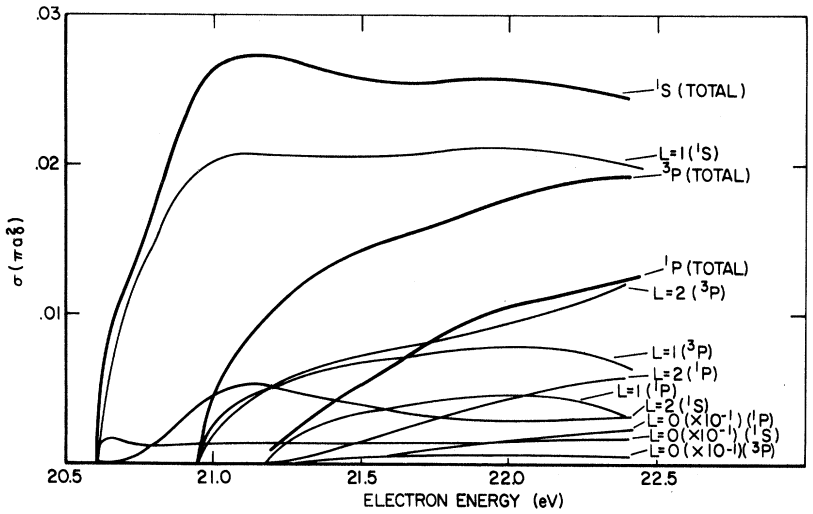

FIG. 15. The $2\,^1S$, $2\,^3P$, and $2\,^1P$ excitation cross sections and their $L=0$, 1, and 2 contributions.

calculated $L=0$ component of these cross sections is extremely small. A better calculation for $L=0$ is not expected to increase significantly the $L=0$ components of these cross sections.

5. POLARIZATION OF $2\,^3P$ and $2\,^1P$ EXCITATION BY ELECTRON IMPACT

The polarization of light emitted by excitation to the $2\,^1P$ or $2\,^3P$ state followed by decay to the $2\,^1S$ or $2\,^3S$ state can be computed from our T-matrix elements for $2\,^1P$ and $2\,^3P$ excitation. For photons emitted perpendicular to the incident electron beam the polarization fraction P will be[40]

$$P=(1-x)/(1+x), \quad {}^1P \text{ excitation},$$

$$P=15(1-x)/(41+67x), \quad {}^3P \text{ excitation},$$

where $x=Q_1/Q_0$, and Q_1 and Q_0 are the cross sections for excitation of $2\,^1P$ or $2\,^3P$ into $m=\pm 1$ or $m=0$ states, respectively. These cross sections can be obtained from the paper by Burke *et al.*[41] [see[42] Eq. (8)].

In Fig. 16 we show the polarization fractions for $2\,^1P$ and $2\,^3P$ excitation. As in the previous section the $L=0$ components of the T-matrix elements used in this calculation have been scaled by a factor of $1/\sqrt{10}$.

Figure 16 may not be an accurate estimate of the polarization fraction for excitation of the $2\,^3P$ and $2\,^1P$ states since the results are expected to be sensitive to the $L=0$ component of our T-matrix elements. We include it merely to point out that the resonant structure below the $2\,^3P$ and $2\,^1P$ threshold has a marked influence on the polarization of impact radiation arising from these states and that the rapid drop of polarization from its threshold value within a few electron volts of threshold is to be expected. Physically, the reason for this is quite clear. At threshold only excitation to $m=0$ states can occur and consequently $x=0$. However, the presence of ^2P and ^2D resonances below the threshold means the $L=1$ and 2 partial waves make large contributions to the scattering cross section near threshold and the excitation of $m=\pm 1$ is quite likely in the near threshold region.

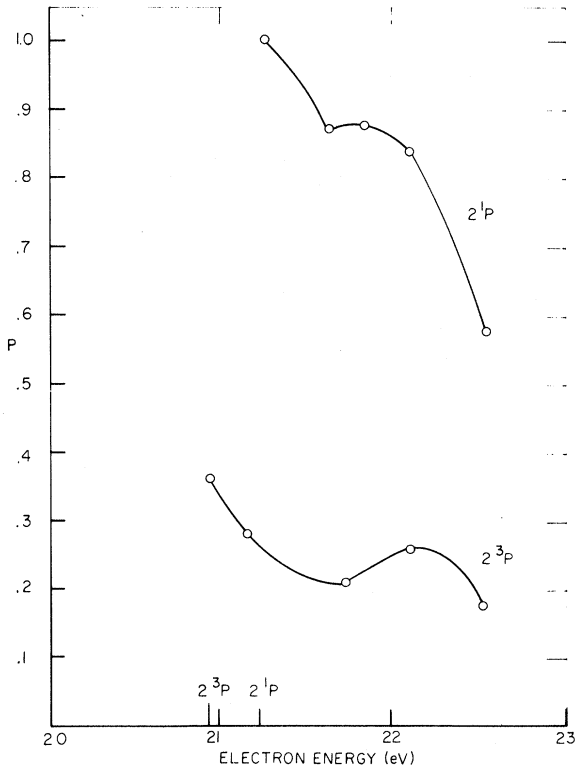

FIG. 16. The polarization fraction versus electron energy for $2\,^3P$ and $2\,^1P$ excitation.

In spite of the uncertainties in our estimates of the polarization fraction the results of Fig. 16 show reasonably good agreement with a recent measurement of polarization for $2\,^3P$ excitation.[43] In this work the polarization was found to fall from its threshold value to a minimum of about 16% before rising to a second maximum at about 1.2 eV above threshold as indicated by our calculation.

6. RESONANCES

A fundamental difficulty in our analysis results from the long-range multipole interactions inherent in the coupling which provides the basic interaction which produces resonances. If the 2^3S and 2^3P states were degenerate then, since the $n=2$ states of He are close to hydrogenic, the dipole coupling between these levels would bind the incident electron into an infinite series of "dipole" states for $L=0$, 1, and 2. These states would produce resonances in the elastic scattering of electrons on the 1^1S state of helium below the $n=2$ threshold. A similar argument also applies to the 2^1S and 2^1P states. Gailitis and Damburg[14] derived an effective range theory which, taking into account the degenerate dipole coupling, predicted the resonance spectrum and the threshold behavior of the excitation cross sections. In helium, however, this degeneracy is broken by ~1 eV and the Gailitis-Damburg theory no longer applies. In Fig. 17 we show a plot of the expected movement of the poles in the S matrix in the complex energy plane as the degeneracy between the $2s$ and the $2p$ states is gradually broken. The $2s$ and $2p$ thresholds are branch points with branch cuts chosen conventionally to run along the real axis to $E=+\infty$. The physical region is along the upper edge of the branch cut (see, for example, Eden and Taylor.[44]) The path of the pole which moves along the real axis is displaced above the axis for clarity and moves as shown round the $2s$ branch point in a clockwise direction onto a nonphysical sheet of E as shown in the figure. When the pole is at A (corresponding to a state bound to the $n=2$ channels) it will mainly affect the elastic scattering cross section on the ground state (not shown in Fig. 17). However, when it has moved to the position B corresponding to a resonant state it will strongly affect the excitation cross section to the $2s$ state. Of course, there may be more than one pole playing an important role since, according to the Gailitis-Damburg theory, the threshold is an accumulation point of an infinite number of poles in the degenerate case.

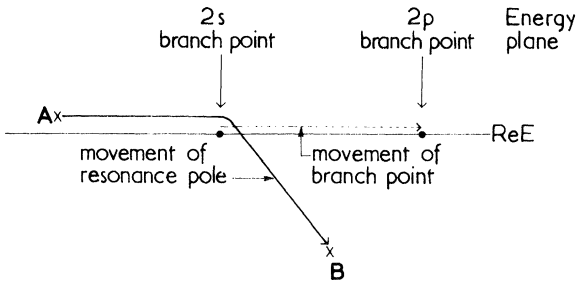

FIG. 17. The expected movement of a resonance pole (denoted by X) in the S matrix as the degeneracy of the $2s$ and $2p$ threshold is broken. The angular momentum is assumed to be greater or equal to one.

Although for e^- – He scattering there is no simple equivalent to the effective range theory of Gailitis and Damburg, we can derive some interesting relations which aid in understanding our results. Brenig and Haag[45] show that the open channel S matrix can be written generally in the neighborhood of an isolated resonance as

$$\underline{S} = \underline{S}_0 - i\Gamma \frac{\underline{S}_0^{1/2}\underline{\gamma}\times\underline{\gamma}\underline{S}_0^{1/2}}{E-E_\gamma+i\Gamma/2}\,, \tag{15}$$

where $\underline{S}_0$ is the nonresonant background S matrix which is assumed to vary slowly in the neighborhood of the resonance pole at $E=E_\gamma-i\Gamma/2$. Here E_γ is the position of the resonance, Γ is its width, and $\underline{\gamma}$ in Eq. (15) is normalized to unit length and gives the fractional width of the resonance for decay into each channel. We now introduce the unitary matrix $\underline{U}_0$ which diagonalizes $\underline{S}_0$, and $\underline{U}$ which diagonalizes $\underline{S}$;

$$\begin{aligned}\underline{U}_0^\dagger\underline{S}_0\underline{U}_0 &= \exp(2i\underline{\delta}_0),\\ \underline{U}^\dagger\underline{S}\,\underline{U} &= \exp(2i\underline{\delta}(E)).\end{aligned} \tag{16}$$

The elements of the diagonal matrices $\underline{\delta}_0$ and $\underline{\delta}(E)$ are the eigenphases of the respective S matrices. If we define a vector y by

$$\underline{y} = \underline{U}_0^\dagger\underline{\gamma}\,, \tag{17}$$

one can show[46] that the eigenphases satisfy the following relation

$$E-E_j = \tfrac{1}{2}\Gamma\sum_{i=1}^{n} y_i^2\cot[\delta_{0i}-\delta_j(E)], \qquad \text{for all } j\,, \tag{18}$$

where n is the number of open channels and where $\delta_j(E)$ is any one of the eigenphases at the energy E. Equation (18) is just the multichannel analog of the single-channel formula used by Burke and McVicar.[47] It follows that the eigenphases are continuous through a resonance and their sum increases by π rad. In the case of a narrow resonance the eigenphases have the structure shown in Fig. 18. This is an example taken from recent work by Burke, Ormonde, and Whitaker[11]

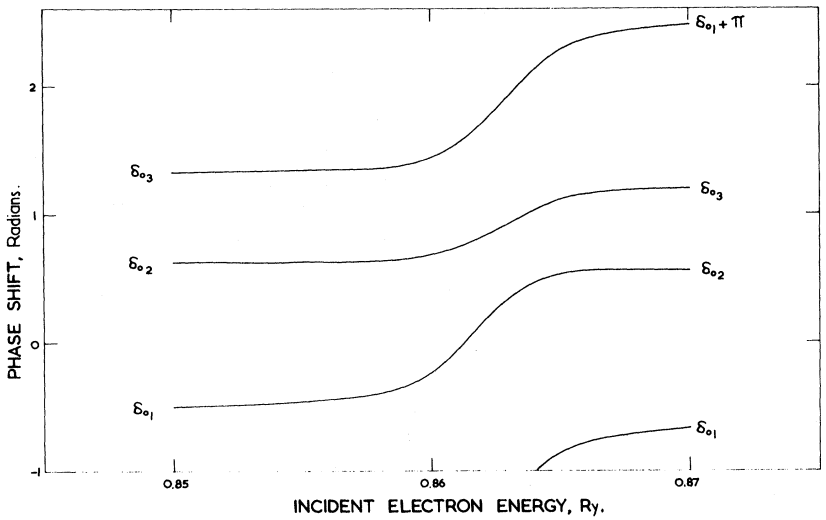

FIG. 18. The ^1S eigenphases near a resonance below the $n=3$ threshold for e^--H scattering. This figure illustrates the behavior of the eigenphases for multichannel scattering.

on e^- – H scattering below the $n=3$ threshold. Note that the eigenphase associated with a particular eigenvector below the resonance (denoted by the subscript on the eigenphase in the figure) becomes associated with the higher eigenvector above the resonance. The crossover effect is analogous to that occurring in the theory of adiabatic molecular potential curves.[48]

The situation for e^- – He is not so simple. In this case the resonances which lie between or above the $n=2$ thresholds are broad compared with the distance in which the background eigenphases change appreciably. Further, the threshold behavior of the background eigenphases is not known owing to the long-range nature of the interaction. We show in Fig. 19 the eigenphases for the ^2S, ^2P, ^2D, and ^2F states from the Set B computations. The first ^2S eigenphase at the $2\,^3S$ threshold is shown going to π rad which is consistent with the presence of the resonance just below the $2\,^3S$ threshold. The threshold behavior of the second ^2S eigenphase, which starts at the $2\,^1S$ threshold, indicates that the S matrix contains a pole close to the $2\,^1S$ threshold. This pole probably arises from the strong coupling between the $2\,^1S$ and the $2\,^1P$ channels and appears on the second sheet of the energy plane. Since, however, there is no angular momentum barrier in this case the pole probably occurs close to or on the real energy axis but below the threshold. (This situation is analogous to the singlet deuteron pole in n-p scattering.[49]) We find that this virtual state strongly enhances the $2\,^3S$-$2\,^1S$ metastable conversion cross section close to threshold but since its position depends sensitively on the approximation used in the solution of the equations, our S-wave results may not be very accurate close to this threshold.

Turning now to the results for higher partial waves we see that the first ^2P eigenphase rises linearly with energy between the $2\,^3S$ and $2\,^1S$ thresholds. In this energy region only one channel is open and in this channel the long-range interaction is determined by the coupling between the $2\,^3S$ and $2\,^3P$ states. This produces an effective αr^{-4} term in the interaction potential with the polarizability α given by

$$f_{2\,^3S,2\,^3P}/(E_{2\,^3P}-E_{2\,^3S})^2 ,$$

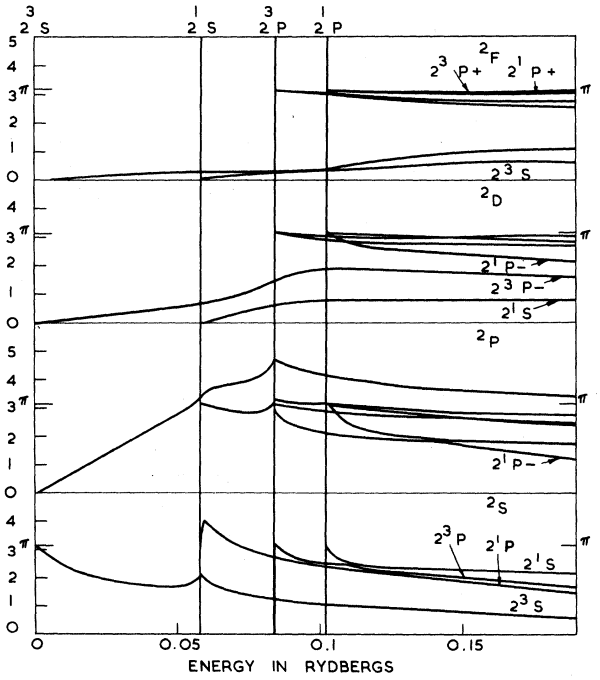

FIG. 19. The ^2S, ^2P, ^2D, and ^2F eigenphases for e^--He scattering from the Set B computations. The notation $2p\pm$ means the $2p$ state with $l_2=L\pm1$. If an eigenstate is dominated by a single channel at the higher energies then the corresponding eigenphase is labeled accordingly.

where $f_{2^3S,2^3P}$ is the oscillator strength of the transition. In this case O'Malley *et al.*[50] show that the phase shift for $l \geq 1$ satisfies the equation

$$\tan\delta_l(k^2) = \pi\alpha k^2/8(l+\tfrac{3}{2})(l-\tfrac{1}{2}) + \text{higher-order terms}, \quad (19)$$

where l is the angular momentum of the incident electron and k^2 is its energy in Rydbergs. Substituting the polarizability of the 2^3S state ($313a_0^3$) into Eq. (19), we find

$$\tan\delta_1(k^2) = 64.2k^2 \ , \qquad \tan\delta_2(k^2) = 9.1k^2 \ . \quad (20)$$

These slopes agree very well with the detailed calculations shown in Fig. 19. In the ^2P case the phase shift is approximately linear in k^2 right up to the $2\,^1S$ threshold by which time the phase shift has increased by over π rad. This linear behavior over an extended energy range does not follow automatically from the threshold law [Eq. (19)] and must be due to an additional feature of the interaction. The rise of the phase shift through $\frac{1}{2}\pi$ indicates that there must be a resonance. Its width and position are not well determined from this data since we are not certain how to unfold the threshold behavior of the phase shift from the resonant behavior. However, if we define the position of the resonance as the energy where the phase shift passes through $\frac{1}{2}\pi$ rad and take the slope at this point to define Γ we find $E_\gamma \approx 20.2$ eV and $\Gamma \approx 0.4$ eV.

In the ^2D case the phase shift rises with a considerably smaller slope from the $2\,^3S$ threshold in agreement with Eq. (20). In this case also the phase shift resonates but not until the energy is above the $2\,^1S$ threshold. Since the corresponding S matrix is here multidimensional, we must make use of Eq. (18) in interpreting the results. We have seen, for example, in Fig. 18, that the sum of the resonant part of the eigenphases increased by π rad as the energy increases through the resonance. At the same time as the resonant eigenphases are increasing, the background eigenphases which start from the $2\,^3P$ and $2\,^1P$ thresholds are strongly decreasing. The result of these two effects is to give a sum which increases by an amount considerably less than π rad. Figure 19 clearly shows the crossover effects mentioned in connection with Fig. 18. The eigenphases in Fig. 19 are labeled by the dominant contribution of the corresponding eigenvector at the highest energy shown. For example, we have found that for ^2D scattering the eigenphase which starts from the $2\,^3S$ threshold becomes mainly $2\,^3P$ after the resonance while the eigenphases which start out from the $2\,^3P$ and $2\,^1P$ thresholds contain the largest component of the $2\,^3S$ state. The position and width of the ^2D resonance are also not well determined. We estimate that the position $E_\gamma \approx 21.0$ eV and width $\Gamma \approx 0.5$ eV.

Finally in Fig. 19 we give the ^2F eigenphases. Again the long-range interactions cause the eigenphases starting from the $2\,^3S$ and $2\,^1S$ thresholds to start linearly with energy, and again the eigenphases resonate but not until the energy is above all the $n=2$ thresholds. We estimate that in this case $E_\gamma \approx 22$ eV and $\Gamma \approx 1$ eV. We summarize the He^- states in Fig. 20. We see a hierarchy of levels of increasing width (the width is indicated in the figure by the shading), angular momentum, and energy. This is analogous to the situation for single-channel scattering discussed by Regge[51,52] who showed that the position of a pole in the S matrix in the complex angular momentum plane l was an analytic function of the energy. Regge showed that in general a pole which gives rise to resonances moves along a trajectory in the first quadrant of the complex angular momentum plane. As the energy increases the pole first moves to the right with a small imaginary value of l. Each time it passes close to an integer value of l it gives rise to a resonance. Eventually for large energies the pole returns to the left half plane with a large imaginary value of l. In the e^--He case resonances are calculated for the ^2S, ^2P, ^2D, and ^2F states. There are indications of broader resonances for states of higher angular momenta at higher energies. However, the situation at these higher energies is not clear since the omitted coupling with the $n=3$ levels will be important.

We discuss finally the time delay associated with these resonances. This concept was introduced by Wigner[53] who showed that the time delay could be expressed in terms of the S matrix by the relation

$$\underline{Q} = i\hbar \frac{d\underline{S}}{dE}\underline{S}^\dagger \ , \quad (21)$$

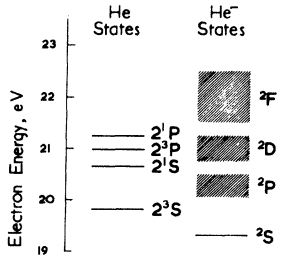

FIG. 20. The level structure of He and He^- over 20 eV. The energy is measured relative to the ground state of He. Numerical energy differences (see Table I) have been used for the $n=2$ levels of He, but the $2\,^3S$ level has been fixed at its experimental value of 19.81 eV.

where $\underline{S}^{\dagger}$ is the Hermitian conjugate of the S matrix. For the case of an isolated resonance in elastic scattering the time delay has a simple physical significance. In this case it can be written as

$$Q = \hbar\Gamma/[(E - E_{\gamma})^2 + (\Gamma/2)^2] \ , \tag{22}$$

and the average time delay of a scattered beam is $2\hbar/\Gamma$ corresponding to the formation and decay of a metastable state with decay lifetime $\hbar/\Gamma$. Smith[54] has generalized this to the situation where several channels are open. In this case for an isolated resonance we can assume that the S matrix can be expressed by Eq. (15). If the background S matrix is assumed to be independent of the energy then the time-delay matrix becomes

$$\underline{Q} = \hbar\Gamma \frac{\underline{S}_0^{1/2}\underline{\gamma}\times\underline{\gamma}\underline{S}_0^{-1/2}}{(E - E_{\gamma})^2 + (\Gamma/2)^2} \ . \tag{23}$$

Diagonalization of this matrix shows that only one of its eigenvalues increases strongly near the resonance while all others stay small. This is a simpler situation than we found when we diagonalized the S matrix where in general all the eigenphases change as the energy increases through the resonance energy. We may therefore hope, by considering the eigenvalues of the time-delay matrix, to see more clearly the resonance structure of the solutions. This hope is borne out in Figs. 21, 22, and 23, which show the eigenvalues of the time-delay matrix determined from our S-, P-, and D-wave solutions, including the ground state in the close-coupling equations. We see that in each case one time delay (labeled 0 in each case) is, with the exception of the rise in $L = 0$ below the $2\,^3S$ threshold, close to zero. These curves correspond to the time delay in elastic scattering from the ground state and reflect the weak coupling between the ground and the excited states. The figures show the time delay produced by the effect of the polarization discussed earlier. If the behavior of the phase shift is given by Eq. (19), then the corresponding time delay is

$$Q_l = 2\pi\alpha/8(l + \tfrac{3}{2})(l + \tfrac{1}{2})(l - \tfrac{1}{2}) \ . \tag{24}$$

These values are computed using the known polarizabilities of the $2\,^3S$ and $2\,^1S$ states and are shown in Figs. 22 and 23. Besides time delays associated with the S-, P-, and D-wave

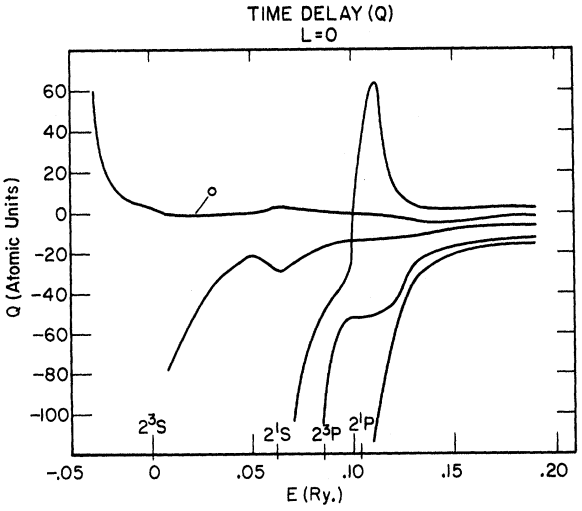

FIG. 21. The eigenvalues of the time-delay matrix (in atomic units) for $L = 0$.

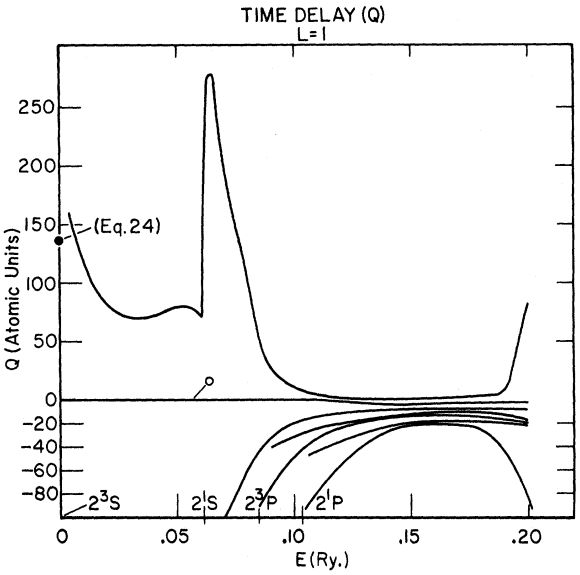

FIG. 22. The eigenvalues of the time-delay matrix (in atomic units) for $L = 1$.

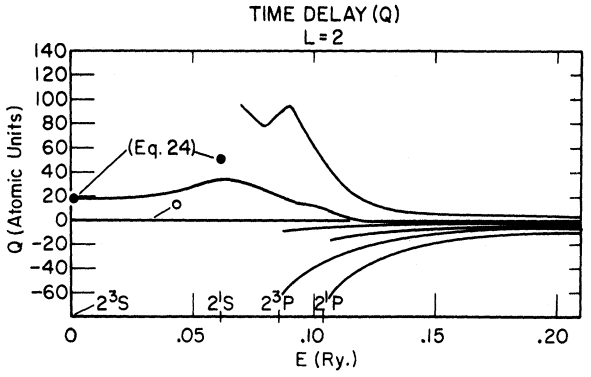

FIG. 23. The eigenvalues of the time-delay matrix (in atomic units) for $L = 2$.

resonances discussed earlier, we now see a further effect. This is an increase in the time delay when a new threshold opens. This effect is evident at the $2\,^1S$ threshold in Figs. 21 and 22. In the S-wave case, this corresponds to the virtual state discussed earlier, however, the P-wave result is new and indicates the possible existence of a virtual state close to the $2\,^1S$ threshold in this case.

The time delays starting at all thresholds above the resonance region in each case are large and negative and decrease rapidly in magnitude as the energy increases. Physically this means that in the representation where Q is diagonal, the eigenstates corresponding to these negative time delays tend to be small near the atom. Also the negative time delays starting from the $2\,^3P$ and $2\,^1P$ thresholds are larger in magnitude for the small l values. This behavior is similar to that produced by hard-sphere scattering.

We conclude this section on resonances for the e^--He system by remarking that our results show the general trend for many situations involving the scattering of electrons from excited atoms. We expect that quite often the dipole coupling term in the interaction will dominate the scattering, and the cross sections close to the thresholds will be influenced by many resonances. The outstanding defect in the theory at present is the absence of an effective range formalism similar to the Gailitis-Damburg theory for degenerate levels that will allow this behavior to be predicted in detail.

7. CONCLUSIONS

In this paper we have presented the theory and results of a calculation of the low-energy scattering of electrons by helium. Our aim has been to investigate the important physical features of the collision problem in the neighborhood of the $n=2$ threshold by comparing our results wherever possible with the detailed experimental data now available in this energy region. We justify our procedure of expanding the total wave function in eigenstates of the target Hamiltonian and retaining just the $1\,^1S$, $2\,^3S$, $2\,^1S$, $2\,^3P$, and $2\,^1P$ states of helium firstly by general theoretical arguments based on the strong coupling of the $n=2$ states, one with another, and secondly by comparison with experiment.

Theoretically, we expect that the large polarizability of the $2\,^3S$ and $2\,^1S$ states will be extremely important both for excitation from the ground state and for electron scattering and metastable conversion between the excited states. Our method of including essentially the full polarizability by the inclusion of the $2\,^3P$ and $2\,^1P$ states in the close-coupling expansion is essential for highly polarizable systems since firstly the solution satisfies a variational principle and secondly it obeys the correct boundary conditions throughout the energy range considered. Our results show that the polarizability is of fundamental importance and plays an important role in producing resonances close to the thresholds.

The resonances found in our calculations are in good agreement with experiment. We find a very good value for the position of the ^2S resonance below the $2\,^3S$ threshold, and we show that the excitation cross sections from the ground state are dominated by ^2P and ^2D resonances. These assignments are in accord with recent experimental angular distribution data. Our calculation has failed to predict the width of the ^2S resonance below the $2\,^3S$ threshold. We find a value about 4 times greater than experiment and our ^2S excitation cross sections from the ground state are correspondingly in error by an amount which may be up to a factor of 10 too large at the highest energy we considered. We attribute this failing to an approximation, necessitated by numerical expediency, which we made in the exchange integrals. Fortunately this error is only significant in the S-wave range, and the dominant P-wave, D-wave, and higher wave contributions give satisfactory agreement with experiment. Thus if we renormalize our S-wave data we find good agreement with experimentally measured cross sections. Further evidence concerning the general validity of our results comes from an analysis of the observed polarization of the impact radiation from the $2\,^3P$ state.

The transitions between the $n=2$ states are not affected by the approximations made in the exchange terms essentially because these transitions are strong, unlike the $n=1-2$ transitions and are less affected by small changes in the interaction. Our results for these transitions are in good agreement with the limited data available and our predictions are expected to be an accurate estimate of these cross sections.

Finally, one difficulty we have had in interpreting and analyzing our data has been that there is not yet an adequate theory of the behavior of cross sections near thresholds in the presence of long-range interactions. The theories applicable when the interactions are short range break down near threshold and attempts to extend the work to long-range forces has only had partial success. We feel that this is an important field of endeavor for future theoretical work.

ACKNOWLEDGMENT

We would like to thank Dr. Ugo Fano for his advice and encouragement through the course of this work.

*Work performed in part at National Bureau of Standards, Washington, D.C., while a guest worker under NATO sponsorship, and in part under a Science Research Council (London) Grant.

†Work supported by the Defense Atomic Support Agency through the Air Force Weapons Laboratory, Kirtland Air Force Base, New Mexico, Contract Nos. AF29(601) 6801 with Lockheed Missiles and Space Company, and AF29(601)-68-C-0052 with Quantum Systems, Inc., Albuquerque, New Mexico.

[1]H. W. S. Massey and E. H. S. Burhop, Electronic and Ionic Impact Phenomena (Clarendon Press, Oxford, England, 1952).

[2]G. J. Schulz and R. E. Fox, Phys. Rev. 106, 1179 (1957).

[3]E. Baranger and E. Gerjouy, Proc. Phys. Soc. (London) A72, 326 (1958).

[4]G. J. Schulz, Phys. Rev. Letters 10, 104 (1963).

[5]For review of the rapidly growing field of resonances in atomic physics, see (a) P. G. Burke, Advan. Phys. 14, 521 (1965); and (b) K. Smith, Rept. Progr. Phys. 29, 373 (1966).

[6]J. Callaway, R. W. Labahn, R. T. Pu, and W. M. Duxler, Phys. Rev. 168, 12 (1968).

[7]H. W. S. Massey and B. L. Moiseiwitch, Proc. Roy. Soc. (London) A 227, 38 (1954); and A 258, 147 (1960).

[8]R. Marriott, in Atomic Collision Processes, edited by M. R. C. McDowell (North-Holland Publishing Co., Inc., Amsterdam, 1964), p. 114.

[9]R. Marriott, Proc. Phys. Soc. (London) 87, 407 (1966).

[10]Preliminary reports of some of the results of these calculations have already been given: (a) P. G. Burke, J. W. Cooper, and S. Ormonde, Phys. Rev. Letters 17, 345 (1966); (b) P. G. Burke, A. J. Taylor, J. W. Cooper, and S. Ormonde, in Proceedings of the Fifth International Conference on Atomic and Molecular Collisions (Nauka, Leningrad, USSR, 1967), p. 376; (c) J. W. Cooper, *ibid.* p. 387.

[11]P. G. Burke, S. Ormonde, and W. Whitaker, Proc. Phys. Soc. (London) 92, 319 (1968).

[12]R. H. Neynaber, S. M. Trujillo, L. L. Morino, and E. W. Rothe, Atomic Collision Processes, edited by M. R. C. McDowell (North-Holland Publishing Co., Inc., Amsterdam, 1964), p. 1089.

[13]A. V. Phelps, Phys. Rev. 99, 1307 (1955).

[14]M. Gailitis and R. Damburg, Proc. Phys. Soc. (London) 82, 192–200 (1963).

[15]J. Macek and P. G. Burke, Proc. Phys. Soc. (London) 92, 351 (1968).

[16]P. M. Morse, L. A. Young, and E. S. Haurwitz, Phys. Rev. 48, 948 (1935).

[17]R. Marriott and M. J. Seaton, Proc. Phys. Soc. (London) A70, 296 (1957).

[18]Actually the ground-state wave function derived by this procedure was not used in any of the calculations reported here. The wave function was obtained in order to have a set of wave functions in analytic form that satisfied the three requirements mentioned in the beginning of this section. However, since this is a poorer approximation than the set generated numerically, the numerical bound-state wave functions were used in all calculations involving the ground state. A word of caution is in order on the use of bound-state wave functions of analytic form in close-coupling calculations; one must be careful that no exponential ξ_i in Eq. (3) is less than the square root of the binding energy. Trial calculations made with bound-state wave functions of the form of Eq. (3), but with exponentials chosen to minimize the total energy for each state ignoring this criterion, led to totally meaningless results due to small oscillations in the bound-state wave functions at large distances.

[19]I. C. Percival and M. J. Seaton, Proc. Cambridge Phil. Soc. 53, 654 (1957).

[20]R. Marriott, Proc. Phys. Soc. (London) A70, 288 (1957).

[21]P. G. Burke and K. Smith, Rev. Mod. Phys. 34, 458 (1962).

[22]G. J. Schulz, in Proceedings of the Fourth International Conference on Electronic and Atomic Collisions (Science Bookcrafters, Inc., Hastings-on-Hudson, New York, 1965), p. 117.

[23]R. W. Labahn and J. Callaway, Phys. Rev. 135, A1539 (1964).

[24]R. T. Pu and E. S. Chang, Phys. Rev. 151, 31 (1966).

[25]D. E. Golden and H. W. Bandel, Phys. Rev. 138, A14 (1965).

[26]E. Holøien and S. Geltman, Phys. Rev. 153, 81 (1967).

[27]D. Husain, A. L. Choudhury, A. K. Rafiqullah, C. W. Nestor, and F. B. Malik, Phys. Rev. 161, 68 (1967).

[28]R. C. Sklarew and J. Callaway, Phys. Rev. 175, 103 (1968).

[29]The $2\,^3S$-$2\,^1P$ cross section reported previously in Ref. 10 (b) is too large by a factor of 3.

[30]M. Inokuti, Y. K. Kim, and R. L. Platzman, Phys. Rev. 164, 55 (1967).

[31]Y. K. Kim, private communication. We thank Dr. Kim for performing this calculation for comparison with our results.

[32]N. F. Mott and H. W. S. Massey, The Theory of Atomic Collisions, (Clarendon Press, Oxford, England, 1965).

[33]F. M. J. Pichanick and J. A. Simpson, Phys. Rev. 168, 1, 64 (1968).

[34]R. J. Flemming and G. S. Higginson, Proc. Phys. Soc. (London) 84, 531 (1964).

[35]The exact width of the 19.3-eV resonance has never been determined. Published estimates are 0.01–0.015 eV [D. Andrick and H. Ehrhardt, Z. Physik 192, 99 (1966)], and 0.01 eV [J. A. Simpson and U. Fano, Phys. Rev. Letters 11, 158 (1963)], and neither estimate takes into account fully the effects of Doppler and instrumental broadening. The estimate of Ref. 10(a) (0.004 eV) was obtained (J. W. Cooper, unpublished) by attempting to unfold these effects from the data obtained by Simpson and Fano.

[36]H. Ehrhardt and K. William, Z. Physik 203, 1 (1967).

[37]H. Ehrhardt, L. Langhans, and F. Linder, Z. Physik 214, 179 (1968).

[38]G. Chamberlain, Phys. Rev. 155, 46 (1967).
[39]We thank Dr. P. G. H. Sandars for suggesting that we examine scattering for angles greater than 90°.
[40]I. C. Percival and M. J. Seaton, Phil. Trans. Roy. Soc. (London) A251, 113 (1958).
[41]P. G. Burke, H. M. Schey, and K. Smith, Phys. Rev. 129, 1258 (1963).
[42]This equation should contain a term $i^{L-L'}$ as has been recently pointed out. P. G. Burke, A. J. Taylor, and S. Ormonde, Proc. Phys. Soc. (London) 92, 345 (1967).
[43]J. H. Whitteker and F. W. Dalby, Can. J. Phys. 46, 193 (1968).
[44]R. J. Eden and J. R. Taylor, Phys. Rev. 133, B1575 (1966).
[45]W. Brenig and R. Haag, Fortschr. Physik 7, 183–242 [English transl.: Atomic Energy Research Establishment Report No. T1066, 1959 (unpublished)].
[46]J. Macek, private communication.
[47]P. G. Burke and D. D. McVicar, Proc. Phys. Soc. (London) 86, 989 (1965).
[48]Reference 31, p. 351 ff.
[49]J. M. Blatt and V. F. Weisskopf, Theoretical Nuclear Physics (John Wiley & Sons, New York, 1952), p. 176.
[50]T. F. O'Malley, L. Spruch, and L. Rosenberg, J. Math. Phys. 2, 491 (1961).
[51]T. Regge, Nuovo Cimento 14, 951 (1959).
[52]T. Regge, Nuovo Cimento 18, 947 (1960).
[53]E. P. Wigner, Phys. Rev. 98, 145 (1955).
[54]F. T. Smith, Phys. Rev. 118, 349 (1960).